ACS OMEGA

Open Access

http://pubs.acs.org/journal/acsodf

Article

Biocompatible Fluorescent Graphene Oxide Quantum Dots for Imaging of *Drosophila melanogaster*

Shiv Rag Mishra, Tuhin Mandal, Surajita Sahu, Monalisa Mishra, Rabi Narayan Senapati, and Vikram Singh*

Cite This: *ACS Omega* 2024, 9, 38916−38924

Read Online

ACCESS | Metrics & More | Article Recommendations | Supporting Information

ABSTRACT: Developing reliable biocompatible bioimaging agents is paramount for diagnosing critical diseases and disorders early through oral ingestion of fluorescent probes to image living organisms. Here, we prepared fluorescent, water-dispersed graphene oxide quantum dots *via* pyrolysis of a *Glycyrrhiza glabra* root in the water medium using a cost-effective and environmentally benign method to enable *Drosophila melanogaster*, an organism analogous to the human genome, to be imaged alive. The prepared graphene oxide quantum dots demonstrated a 2.6 nm diameter and 0.36 nm graphitic spacing with carboxylic acid, carbonyl, and hydroxyl functionalities. The selected area electron diffraction image analysis reveals a series of bright circular patterns that confirm the crystalline nature of the graphene oxide quantum dots. Raman and X-ray diffraction analyses also validate the crystallinity nature of prepared materials. The graphene oxide quantum dots exhibited blue fluorescence under ultraviolet-light irradiation with excitation-dependent emission properties from blue to red emission. The synthesized graphene oxide quantum dots consistently fluoresce in the larva-fed graphene oxide quantum dots without exhibiting toxicity. The current study evaluates the toxic effect of synthesized fluorescent graphene quantum dots by examining several screening and staining methods on *D. melanogaster*, a fruit fly, as a model.

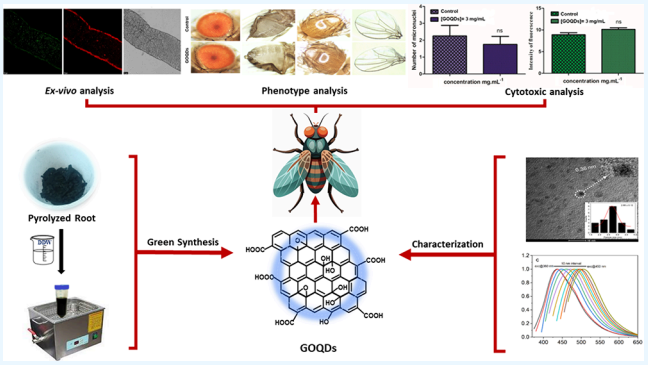

1. INTRODUCTION

Biological imaging has grown to be a potent tool in biomedical research as it provides a unique method for visualizing the morphological characteristics of living organisms. Fluorescent-based imaging has been highly promoted in bioimaging over radioisotope labeling, magnetic resonance imaging, erythrocyte sedimentation rate, and electrochemical detection due to its high sensitivity, high selectivity, convenience, safety, and nondestructive nature.[1,2] In the present scenario, fluorescent carbon nanomaterials (CNMs) received significant attention for biomedical applications over organic dyes, inorganic quantum dots, and up-conversion rare-earth materials due to their biocompatibility, easy to functionalize, water-dispersed, better quantum yield, and tunable emission.[3−12] Various fluorescent CNMs have been reported for *in vivo* fluorescence imaging of biological matrices.[13−17] Among the reported FCNMs, graphene oxide quantum dots (GOQDs) are rarely explored as agents for *in vivo* imaging. The dense sp^2-hybridized carbon atoms with zero-dimensional honeycomb lattices of GOQDs contribute to the exceptional optical properties, making them a promising fluorescent probe for *in vivo* imaging.[18] The synthesis of GOQDs mainly includes the chemical exfoliation of graphite nanoparticles,[19] electrochemical treatment of citric acid,[20] ammonia-treated oxidation of graphene oxide,[21] microwave heating of carbon nanotubes, mixed strong acid oxidation-assisted ultrasonication of graphite nanoparticles,[22] pulse lazar ablation of coal in ethanol,[23] and so forth. Most reported methods are complicated and time-consuming, involving strong chemicals and demanding easy alternative methods.

Drosophila melanogaster, a fruit fly, has an almost similar genome to humans and possesses an analogy to human disorders. *D. melanogaster* is genetically tractable and an ideal *in vivo* model for toxicity and imaging studies due to its short life cycle, diverse mutations, and well-known anatomical position.[24−27]. Thus, different nanomaterials are employed to study and image the *D. melanogaster* organism model. Paithankar et al. investigated the impact of fluorescent cadmium telluride quantum dots on life span, growth, pregnancy, and activity at the organismal level, the reactive oxygen species, and cell death at the subcellular level in *D.*

Received: June 4, 2024
Revised: August 1, 2024
Accepted: August 5, 2024
Published: August 30, 2024

Scheme 1. Graphical Presentation for the Development of Blue-Emitting GOQDs Using Ultrasonication of Pyrolyzed Material of the *G. glabra* Root

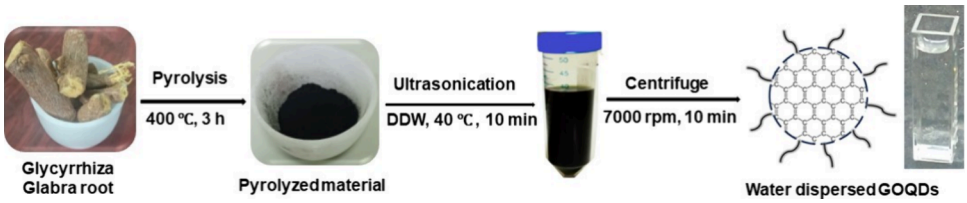

melanogaster.[28] Alaraby et al. reported the exposure of TiO_2 nanoparticles to understand the toxic impact in the *Drosophila* fly model by investigating the genotoxicity, gene expression, and oxidative stress.[29] Agrawal and his co-workers discovered that silver nanoparticles with curcumin exhibited a co-supplemented toxic effect in the tissues of the *Drosophila* larvae by significantly reducing the number of reactive oxygen species and cell death.[30] These materials exhibited toxic effects, complex reaction methods, and high costs compared to those of our proposed materials. Therefore, developing a simple, benign, and cost-effective material to apply as a fluorescent probe for imaging *Drosophila* is essential for understanding the human genome and disorder mechanism.

Recently, fluorescent CNMs have made biomass one of the most significant and sustainable carbon precursors due to their large-scale availability, low cost, and environmentally benign approach. Biomass contains a variety of pre-existing carboxylic, hydroxyl, and amino groups, which facilitate the synthesis of functionalized fluorescent CNMs.[31,32] We have developed a straightforward green synthesis of water-dispersed GOQDs from pyrolyzed readily available biomass *Glycyrrhiza glabra* roots using water-assisted 10 min ultrasonication. The *G. glabra* is enriched with the source of flavonoids, triterpenoids, phenolics, glycosides, and sterols, which are carbonized, aromatized, and later oxidized to get the oxygen-induced honeycomb lattice structure. Further, we investigate the *in vivo* and *ex vivo* studies to understand the genotoxic, neurological, developmental, and morphological aspects of the Oregon-R strain of the *D. melanogaster* fly model using fluorescent GOQDs. The staining images of GOQD-fed larvae demonstrated the exceptional bioimaging capability of fluorescent GOQDs. The study did not find a significant change in DNA damage, and increasing ROS level confirms the noncytotoxic nature of GOQDs. The developmental and morphological investigations on the phenotype of Drosophila further validate the GOQD biocompatibility. These findings raise new hopes for applying GOQDs as diagnostic tools in the biological domain.

2. EXPERIMENTAL DETAILS

2.1. Materials. The *G. glabra* roots (common Indian name: Mulethi) were collected from the local market in Dhanbad, Jharkhand. Whatman 42 filter paper was purchased from Sigma-Aldrich Ltd. Doubled-distilled water was collected from our laboratory. The 4′6-diamidino-2-phenylindole and dichloro-dihydro-fluorescein diacetate were purchased from Sigma-Aldrich, Merck, Germany.

2.2. Instrumentation. A Thermo Fisher Scientific Talos F200X G2, a high-resolution transmission electron microscope (HRTEM), was employed to identify the shape and morphology of these as-prepared GOQDs. A Shimadzu Iraffinity-1s infrared spectrophotometer determined the surface functional groups. The PHI 5000 versa probe III equipment was used to perform X-ray photoelectron spectroscopy to confirm the surface functionalities and the elemental compositions of GOQDs. The 5 eV to 5 keV ion beams using a monatomic argon gun were used to determine the counts per second of various groups as a function of the bonding energy. The absorption and emission studies were carried out by an Agilent Carry 5000 UV−vis−NIR and 150 W xenon lamps consisting of Hitachi F-7000 fluorescence spectrophotometers, respectively. The Raman spectroscopy experiment was conducted using a Horiba Scientific LabRAM HR-UV-Open instrument. A Rigaku Smartlab X-ray diffractometer was used to gather the X-ray diffraction (XRD) patterns.

2.3. Preparation of GOQDs from *G. glabra* Roots. The *G. glabra* roots were cleaned with distilled water to remove dust particles and dried at 70 °C in an oven for 2.0 h. The 10.0 g small pieces of dried *G. glabra* roots were pyrolyzed in a furnace at 400 °C with a heating rate of 5 °C/min for 3.0 h to get the carbonized material. The obtained carbonized materials were crushed thoroughly and collected by sieving them into a fine powder. The 0.5 g portion of fine char powder was taken in 10 mL of double-distilled water, and the mixture was sonicated at 40 °C for 10 min. After ultrasonication, following a Whatman 42 filter paper filtration of the water-dispersed GOQDs and later, the supernatant underwent a 10 min centrifugation at 7000 rpm. Then again, the GOQD solution was purified by a 1.0 kDa dialysis membrane kit for 1 day to remove unreacted large particles. The purified GOQDs (3.0 mg/mL) were stored at 4 °C for further analysis and imaging application (Scheme 1). The calculated product yield of the as-prepared GOQDs was 6%.

2.4. Fly Culture. The experiments were performed by using the Oregon-R strain of *D. melanogaster*. The flies were brought up on an ideal fly medium of sucrose, agar type I, cornmeal, and yeast. The diet was supplemented with methyl-paraben and propionic acid to guard against microbial and fungal contamination. Flies were put into fresh food vials in each experiment at a fixed ratio of five males to seven females. Room conditions were strictly regulated, with a steady 24 °C temperature, a 12 h day−night cycle, and a 60% relative humidity. These conditions were meticulously maintained throughout the investigation to ensure reliable results.

2.5. *Ex Vivo* and *In Vivo* Analysis. Third-instar larvae were utilized throughout the experiment. For *ex vivo* analysis, larvae were cleaned with 1× PBS (phosphate buffer saline). The gut was dissected and kept in 4% paraformaldehyde (PFA) overnight. Following this, the gut was washed with 1× PBS for 10 min, followed by phosphate buffer saline with Tween 20 (PBST) for 10 min, and then stained with GOQDs for 10 min. Finally, using 20% glycerol, the gut was placed on a glass slide and examined under a confocal microscope (Leica-

https://doi.org/10.1021/acsomega.4c05244
ACS Omega 2024, 9, 38916−38924

DMi8, Germany). For *in vivo* analysis, third-instar larvae were washed with 1× PBS and fed with S3M in an Eppendorf tube for 45 min. Then, the gut was dissected and kept in 4% PFA followed by mounting and visualizing under confocal microscopy.

2.6. Evaluation of the Cytotoxic Effect and DNA Damage in the Larval Gut. The larval gut was cautiously dissected, and it was then preserved for an overnight period in a solution containing 4% PFA according to the procedure.[33] Subsequently, the gut was stained with two different compounds: 4′6-diamidino-2-phenylindole (DAPI, catalog no. D9542, Sigma-Aldrich, Merck, Germany) and dichlorodihydro-fluorescein diacetate (DCFH-DA, catalog no. D6883, Sigma-Aldrich, Merck, Germany). DAPI was used in this staining procedure to identify the nuclei of cells specifically, and DCFH-DA was used to examine the generation of reactive oxygen species (ROS) by mitochondria. Washing steps were carried out using 1× PBS.

2.7. Trypan Blue Assay. Third-instar larvae were stained with Trypan blue following a documented protocol.[33,34] The five third-instar larvae were taken separately from both groups (control and GOQDs fed) in 1 mL of an Eppendorf tube. Under dark conditions, these tubes were kept on a rocking shaker (ROCKYMAX) for 30 min. After that, it was washed with 1× PBS for 10 min to prevent overstaining.

2.8. Larva-Crawling Assay. A previously published protocol was used to observe the crawling behavior of the larvae.[33,34] Agarose solution (180 mL, 2%) was prepared and poured into six Petri plates equally. Third-instar larvae, one by one, were placed at the center and allowed to crawl until they reached the edge of the Petri plates. Their paths were traced using a marker. Graph paper was utilized as a scale to measure the crawling speed of larvae in mm/s.

2.9. Phenotype Analysis. Third-instar larvae underwent metamorphosis to transform into an adult. The 30 adult flies were considered and examined under a stereomicroscope (Motic-SMZ171). The eye, wing, thorax, and abdomen morphology were carefully analyzed.[33]

3. RESULTS AND DISCUSSION

3.1. Morphology and Topography. The HRTEM analysis examined the size and morphology of the ultrasonication-assisted precarbonized *G. glabra* root-derived GOQDs. The as-prepared GOQDs exhibited a sphere-like shape and evenly distributed in the water medium (Figure 1a). Figure 1b of the HRTEM image shows a high crystallinity nature of GOQDs having a distinct lattice structure with an interplanar spacing of 0.36 nm, matching the (002) facet of graphitic carbon. The size distribution plot (inset, Figure 1b) confirmed the average diameter of the GOQDs found to be 2.6 nm. The successive bright circular patterns were seen in the selected area electron diffraction (SAED) image, further confirming the crystalline nature of the GOQDs (Figure 1c). The formation of the respective elements is determined using scanning transmission electron microscopy (STEM) and the associated energy-dispersive X-ray spectroscopy (EDS) investigation. It is discovered that carbon and oxygen are evenly distributed, with carbon outweighing the other components (Figure S1 in the Supporting Information). The combined elemental mapping of carbon and oxygen is shown in Figure 1d, which demonstrates how these elements are uniformly distributed throughout the GOQDs at smaller particle sizes.

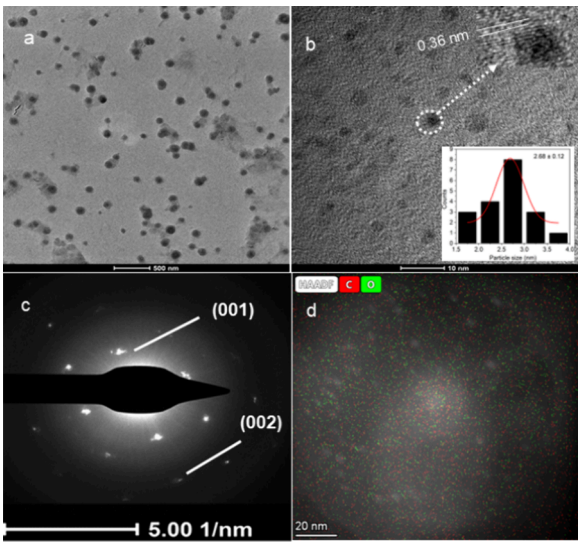

Figure 1. Transmission electron microscopic and scanning transmission electron microscopic images of GOQDs derived from the *G. glabra* root (a) under 500 nm magnification and (b) under 10 nm magnification with the lattice plane distance and particle size distribution plot in the inset. (c) SAED image showing a bright consecutive ring pattern and (d) combined carbon and oxygen EDS and STEM mapping.

The crystalline nature of GOQDs was further explored by using XRD and Raman spectroscopy. The Raman spectroscopic data of GOQDs (Figure 2b) verify two characteristic peaks at 1343 and 1576 cm^{-1}, indicated to the D and G bands, respectively.[35] The primary cause of the D and G peaks is thought to be vibrations of bent carbon atoms in the disordered carbon structure. The intensity ratio between the disordered D and the crystalline G bands (I_D/I_G) is approximately 1.04, suggesting that GOQDs have a highly crystalline graphitic structure. The XRD analysis was used in addition to Raman spectroscopy to describe the graphitic nature of GOQDs (Figure 2a). The characteristic graphitic 2θ peaks were observed at 14.4, 24.5, 29.5, and 38.2°, which correspond to the planes (001), (002), (020), and (200), respectively, for GOQDs.[36] An intense peak is observed at 2θ = 24.5°, attributed to an interlayer spacing of 0.36 nm, which is the signature for graphite (002) planes in GOQDs. The increase in the interlayer spacing is due to oxygen-containing functional groups.

3.2. Surface Functionality. The surface functionalities of the as-prepared GOQDs were examined by using FTIR and XPS techniques. Two major bands were seen at 284.4 and 530.4 eV, which correspond to C 1s and O 1s with atomic percentages of 79.40 and 18.77%, respectively, in the XPS survey analysis of GOQDs (Figure 3a). The binding energy values of the different functional groups were identified by obtaining the full scan spectra of C 1s and O 1s. The high-resolution scan of the C 1s region confirms the three distinct chemical environments of carbon, matching to bond energies of C═C at 283.9 eV, C−OH/C−C at 285.6 eV, and CO at 287.7 eV (Figure 3b). Peaks attributable to C═O at 531.0 eV, C−OH at 532.4 eV, and O—C═O at 532.9 eV are evident of the deconvoluted O 1s spectra (Figure 3c). The presence of different surface functionals at the surface of GOQDs was further supported by FTIR analysis (Figure 3d). The stretching frequency at 3310 cm^{-1} corresponds to the alcoholic groups

https://doi.org/10.1021/acsomega.4c05244
ACS Omega 2024, 9, 38916−38924

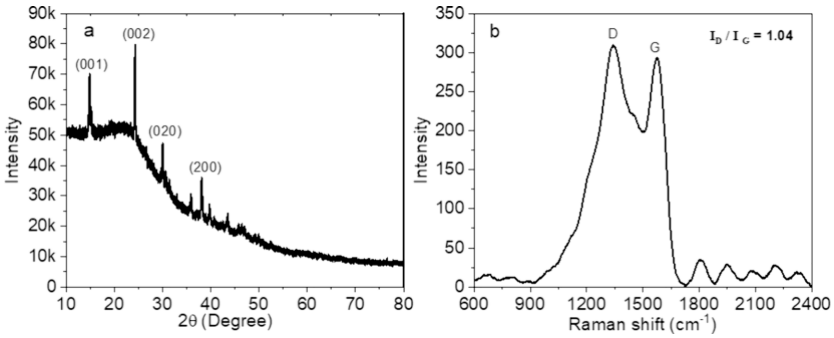

Figure 2. Presentation of (a) Raman and (b) XRD spectra of GOQDs obtained from pyrolysis of the *G. glabra* root.

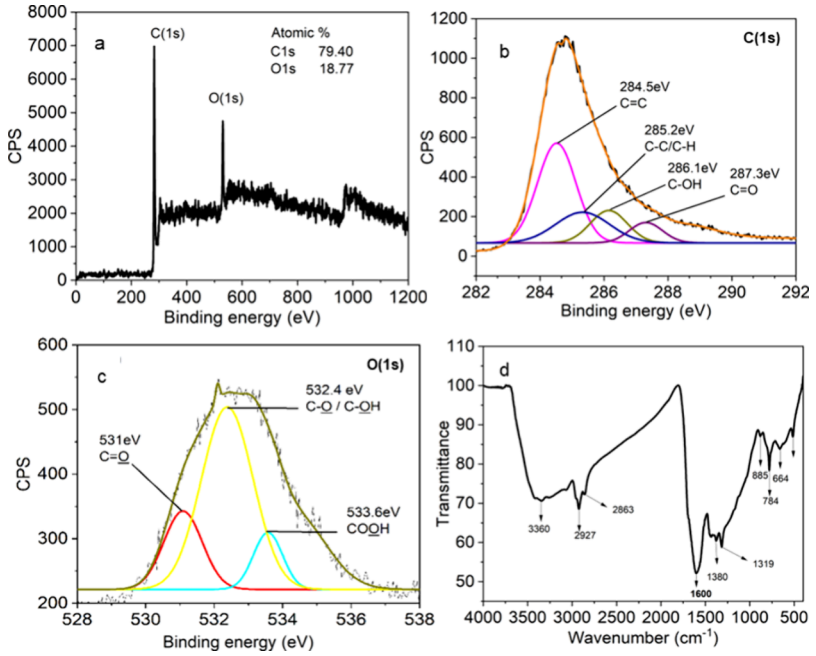

Figure 3. (a) Full scan of the XPS survey spectra with the atomic percentage of GOQDs; (b) high-resolution C 1s full spectrum; (c) high-resolution O 1s full spectrum; (d) FTIR spectra of GOQDs.

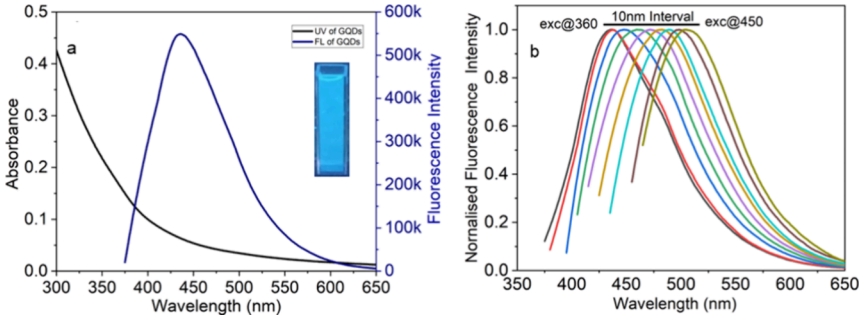

Figure 4. (a) Spectrum of the absorption and emission with the inset showing the blue fluorescent image GOQDs (λ_{exc} = 370 nm and λ_{em} = 435 nm). (b) Normalized excitation-dependent emission spectra of GOQDs in an aqueous medium [GOQDs] = 3.0 mg/mL.

and the band at 1600 cm^{-1} matches the stretching vibration of C═C. The band at 1320 cm^{-1} may be due to the coupled vibration of C−O stretching and O−H bending. The characteristic bands at 2927 and 2853 cm^{-1} correspond to sp^2 and sp^3 C−H stretching vibration modes, respectively.[37] The presence of sp^2- and sp^3-bonded carbon atoms verifies that the synthesized GOQDs are a two-dimensional form of graphene oxide (Figure 3d). The XPS and FTIR investigations confirmed that the carbonyl, hydroxyl/epoxide, and carboxylic acid groups are present on the surface of GOQDs.

We have also examined the high-resolution scan of the C 1s and O 1s XPS spectra of charred powder. The XPS scan confirms the presence of hydroxyl functional group in the charred powder (Figure S2 in the Supporting Information). Hence, we can say that carboxyl, carbonyl, and epoxide functional groups in GOQDs are introduced by ultrasonic charred powder treatment in the presence of water.

https://doi.org/10.1021/acsomega.4c05244
ACS Omega 2024, 9, 38916−38924

Scheme 2. Possible Mechanism of the Development of GOQDs *via* the Ultrasonication of *G. glabra* Roots

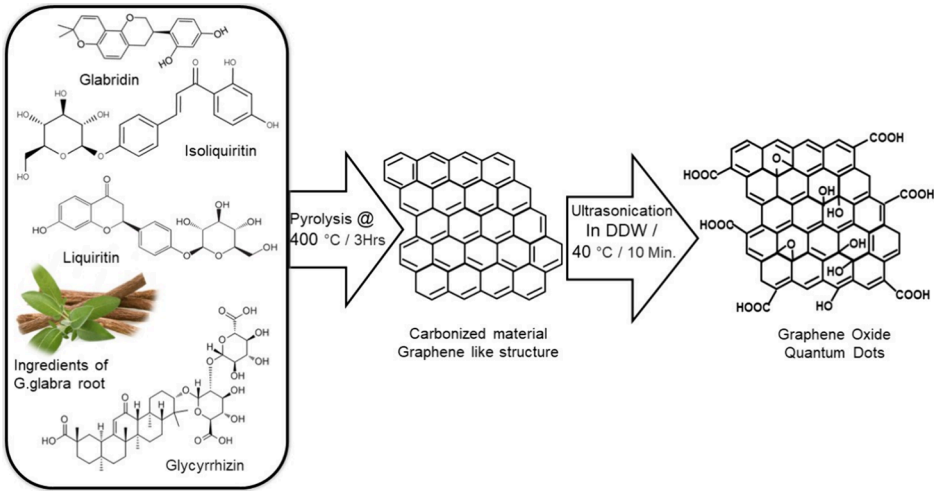

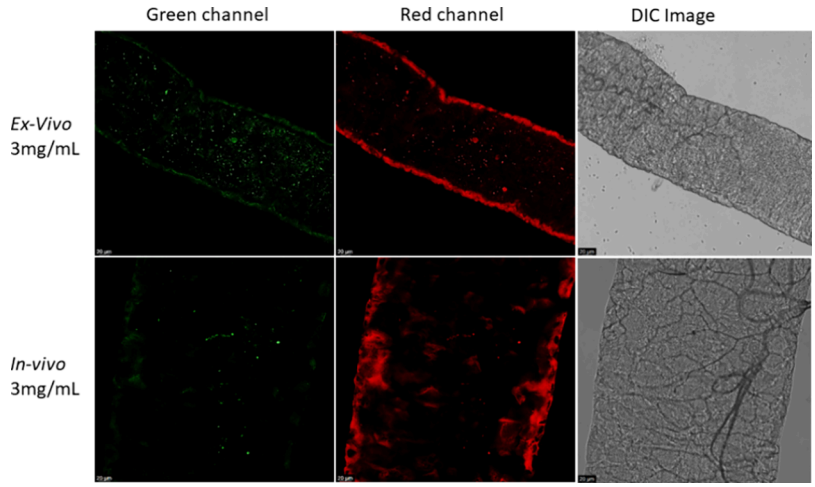

Figure 5. Depicting the fluorescence imaging of the *Drosophila* larva gut tissue in the presence of the GQOD (3.0 mg/mL) concentration. For *ex vivo* and *in vivo* analysis in the green (excitation, 488 nm, and emission, 560 nm) and red channel (excitation, 570 nm, and emission, 700 nm) along with the differential interference contrast (DIC) image.

3.3. Photophysical Study. The photophysical characteristics of the as-prepared GOQDs were examined in a water solution at room temperature. A transparent dispersed solution of 3.0 mg mL^{-1} GOQDs exhibited absorption at approximately 300−550 nm (Figure 4a) with a peak at 300 nm. The absorption band at 300 nm indicates the typical absorption of aromatic π systems or the $\pi-\pi^*$ transition of oxygen-based functional groups, which involves the trapping of excited-state energy by the surface states. The GOQD solution showed intense blue fluorescence (Figure 4a, inset), with the emission peaking at 435 nm (Figure 4a, blue) under 370 nm UV-light exposure. The relative quantum yield of GOQDs is 55% by taking quinine sulfate dye as a standard in water.

To investigate the water-dispersed GOQDs' excitation-dependent emission characteristics, we scanned the GOQD solution at excitation wavelengths between 360 and 450 nm with 10 nm intervals and recorded the emission response between 370 and 650 nm (Figure 4b). The emission spectra showed a noticeable red-shift with the highest intensity at 370 nm excitation (Figure 4b). The presence of varied-sized GOQDs and carboxylic groups on their surface could cause the observable tunability in the normalized emission spectra.

3.4. Mechanism of GOQD Formation from *G. glabra* Roots. Generally, oxygen is linked with functional groups, such as ethers, hydroxyl, phenols, carbonyl, and carboxyl, in biomass feedstocks. In contrast, hydrogen is linked to the surfaces of aromatic structures (aromatic C−H) and aliphatic molecules. Pyrolysis involves breaking covalent bonds of the carbon-bonded heteroatoms and condensing carbon into aromatic structures while releasing structural hydrogen and oxygen. At 400 °C, the C−C bond is reorganized, followed by elimination and dehydration processes. At this point, cyclization and the removal of volatile components cause rapid weight loss, forming the graphene-like structure.[38] Ultrasonic treatment of carbonized material introduces oxygen into the layered structure through carboxyl, carbonyl, hydroxyl, and epoxide functional groups. These oxygen-containing functional groups expand the interlayer gaps within the graphene structure (Scheme 2).

3.5. *Ex Vivo* and *In Vivo* Analysis. The *D. melanogaster* gut tissue was stained with a 3.0 mg/mL GOQD concentration. The images were taken at excitation, 488 nm, and emission, 560 nm, for the green channel. For the red channel, images were taken at an excitation of 570 nm and

https://doi.org/10.1021/acsomega.4c05244
ACS Omega 2024, 9, 38916−38924

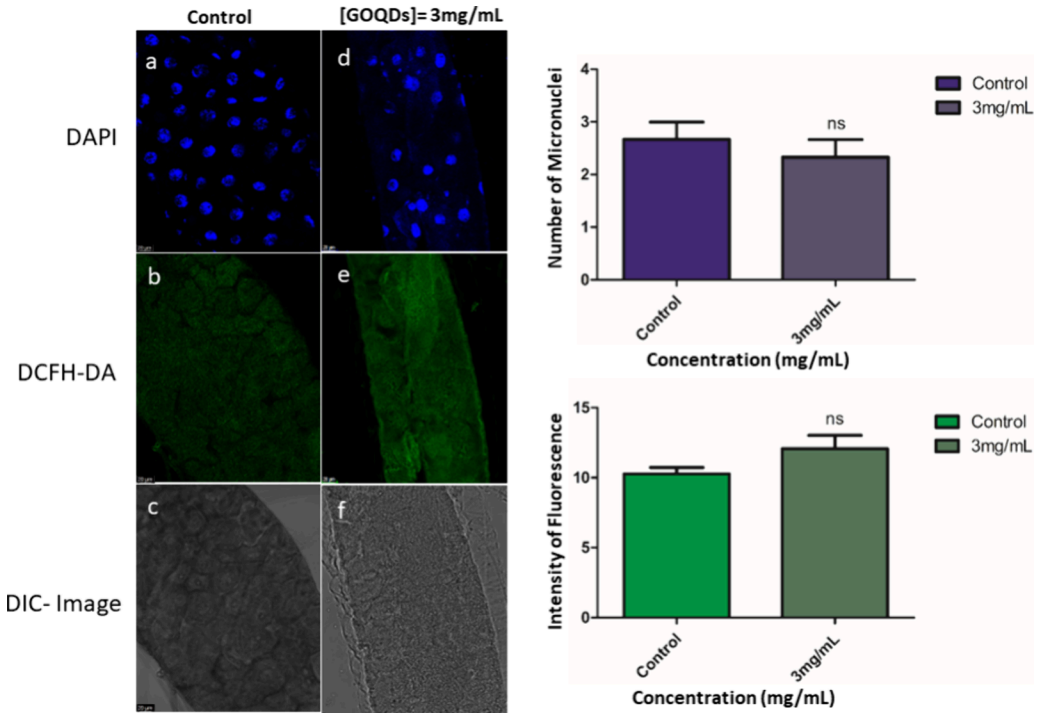

Figure 6. First column represents the control gut (a–c), and the second column represents the GOQD-fed gut with a 3.0 mg/mL concentration (d–f). Figures (a, d) show DAPI staining to find any nuclear damage, parts (b, e) show DCFH-DA staining for ROS estimation, and parts (c, f) represent differential interference contrast (DIC) images.

emission of 700 nm for both *ex vivo* and *in vivo* analysis. *Ex vivo* analysis showed that fluorescence imaging in the gut is seen in both the green and red channels more prominently than *in vivo* imaging. Direct staining of the gut with GOQDs shows a notable response compared to feeding the larva (Figure 5).

3.6. Evaluation of the Cytotoxic Effect and DNA Damage Caused by GOQDs in the Larval Gut. The larvae were fed GOQDs, which passed through the intestinal tract and interacted directly with the gut's epithelial cells. DAPI staining was used to detect any potential DNA damage caused by exposure to the GOQDs, and no DNA damage was observed with a 3.0 mg/mL concentration compared with the control group. DNA damage is considered a marker of genotoxicity,[39] and the absence of DNA damage suggests that GOQDs are nontoxic. A similar nontoxicity was reported when the larvae were fed biscoumarinyl hydrazine and a coumarin-based dye.[15,33] To assess the induction of oxidative stress after ingesting GOQDS, the larval guts were stained with DCFH-DA. The study found no evidence of a substantial rise in mitochondrial ROS levels within the gut following ingestion of GOQDs (Figure 6).

3.7. Trypan Blue Assay. Trypan blue staining was used to distinguish between live and dead cells.[40] No positive Trypan blue stain was observed at 3.0 mg/mL GOQDs, the same as control larvae (Figure 7). This result suggests that GOQDs at 3.0 mg/mL are noncytotoxic.

3.8. Larva-Crawling Assay. Larval movement is governed by muscle contractions regulated by motor neurons (Figure 8).[41] In control larvae, no pause was observed, and they crawled straight at a speed of approximately 1.3–0.9 mm/s. A slight difference was noted at 3 mg/mL concentration GOQDs, where the speed was reduced to 1.06–0.8 mm/s but with a straight crawl. The graph was generated by using Prism GraphPad 5.

Figure 7. Depicting Trypan blue staining of third-instar larva: (a) control and (b) GOQD-fed larvae with 3.0 mg/mL. In the presence of GOQD-fed larvae, no Trypan blue-positive stain was found.

3.9. Phenotype Analysis. The morphology of adult flies, including the eye, wing, thorax, and abdomen, was assessed by using a stereomicroscope (Figure 9). A comparison of the eye phenotype between treated and control flies revealed no abnormalities. The wing venation and shape of treated flies were also typical, similar to normal flies, indicating normal development. Additionally, no bristles or thoracic region damage was observed at any concentration. The absence of phenotypic defect suggests that GOQDs do not affect any pathway associated with the development of Drosophila.

4. CONCLUSIONS

In conclusion, a simple, straightforward 10 min ultrasonication synthesis method was performed to develop the water-dispersed GOQDs from a pyrolyzed *G. glabra* root. The synthesized GOQDs are 2.6 nm in diameter and 0.36 nm in graphitic spacing with carbonyl, hydroxyl, and carboxylic acid functionalities on the surface. The HRTEM analysis confirmed

https://doi.org/10.1021/acsomega.4c05244
ACS Omega 2024, 9, 38916–38924

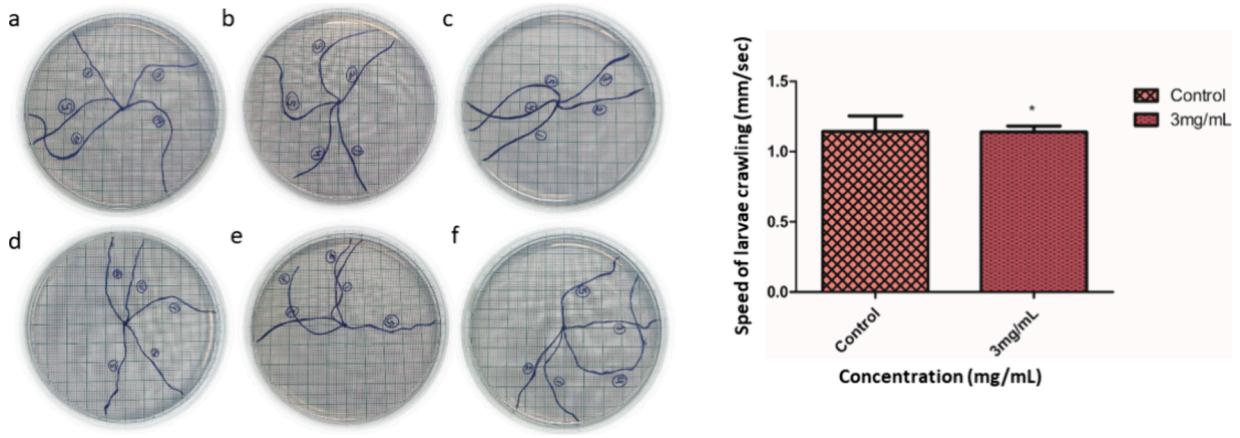

Figure 8. Showing the crawling pattern for control larvae (a–c). The larva crawls in a straight path with an average speed. In GOQD-fed larvae (d–f), there are turns in larvae's crawling patterns with significantly reduced speed.

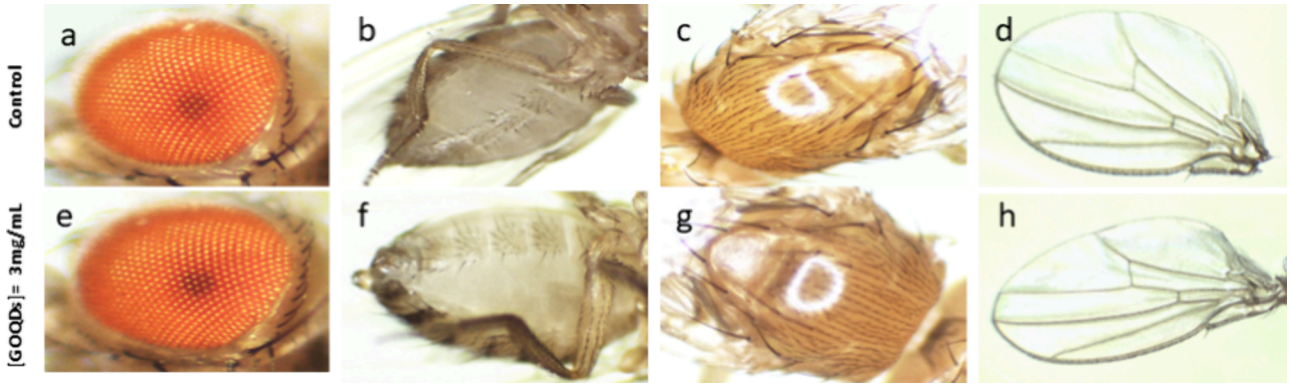

Figure 9. Showing the phenotype of control flies (a–d) and GOQD-fed flies (e–h).

the spherical morphology and crystalline nature of GOQDs. A further investigation using Raman and XRD supported the GOQDs' crystallinity. The STEM and EDS analysis validated uniform carbon and oxygen distribution in the dispersed GOQDs. The XPS and FTIR investigations indicate that the GOQDs were functionalized with carbonyl, hydroxyl/epoxide, and carboxylic acid groups. Their outstanding properties, such as small size, biocompatibility, nontoxicity, aqueous solubility, and excitation- and size-dependent PL emission, prompted us to apply GOQDs for bioimaging applications. The GOQDs were checked for their effect on genotoxicity, neurons, and developmental and morphological behavior in the Oregon-R strain of *D. melanogaster*. The *in vivo* and *ex vivo* models revealed no change in ROS levels and DNA damage, suggesting that the GOQDs have no cytotoxic effect. The stained images of larva-fed GOQDs illustrated the remarkable bioimaging potential of fluorescent GOQDs. The current study proposes that the synthesized GOQDs can be employed in a broad range of biological applications.

■ ASSOCIATED CONTENT

Supporting Information

The Supporting Information is available free of charge at https://pubs.acs.org/doi/10.1021/acsomega.4c05244.

Characterization, EDS images for carbon and oxygen mapping, and XPS spectra of charred powder (PDF)

■ AUTHOR INFORMATION

Corresponding Author

Vikram Singh − *Environment Emission and CRM Section, CSIR-Central Institute of Mining and Fuel Research Dhanbad, Dhanbad, Jharkhand 828108, India; Academy of Scientific and Innovative Research (AcSIR), Ghaziabad 201 002, India;* orcid.org/0000-0003-4283-011X; Email: vikku.010@gmail.com, vikramsingh@cimfr.nic.in

Authors

Shiv Rag Mishra − *Environment Emission and CRM Section, CSIR-Central Institute of Mining and Fuel Research Dhanbad, Dhanbad, Jharkhand 828108, India; Academy of Scientific and Innovative Research (AcSIR), Ghaziabad 201 002, India;* orcid.org/0009-0009-5549-5657

Tuhin Mandal − *Environment Emission and CRM Section, CSIR-Central Institute of Mining and Fuel Research Dhanbad, Dhanbad, Jharkhand 828108, India; Academy of Scientific and Innovative Research (AcSIR), Ghaziabad 201 002, India;* orcid.org/0000-0002-8670-7765

Surajita Sahu − *Department of Life Science, National Institute of Technology, Rourkela, Odisha 769008, India*

Monalisa Mishra − *Department of Life Science, National Institute of Technology, Rourkela, Odisha 769008, India*

Rabi Narayan Senapati − *Environment Emission and CRM Section, CSIR-Central Institute of Mining and Fuel Research Dhanbad, Dhanbad, Jharkhand 828108, India; Academy of Scientific and Innovative Research (AcSIR), Ghaziabad 201 002, India*

https://doi.org/10.1021/acsomega.4c05244
ACS Omega 2024, 9, 38916−38924

Complete contact information is available at:
https://pubs.acs.org/10.1021/acsomega.4c05244

Notes

The authors declare no competing financial interest.

■ ACKNOWLEDGMENTS

V.S. thanks CSIR-Central Institute of Mining and Fuel Research Dhanbad for funding (MLP-155/2021-22; MLP-190/2024-25) and for providing the facilities. S.R.M. thanks Dayanand Vedic College, Orai (Jalaun), for providing the financial support and necessary help. The authors acknowledge the central research facility, the Indian Institute of Technology (ISM) Dhanbad, for the HRTEM, XPS, and UV-visible analyses. The authors also acknowledge Prof. Kaushal Kumar, Physics Department, and Prof. Sumanta Sahu, Chemistry Department, IIT (ISM) Dhanbad for providing a fluorescence facility.

■ REFERENCES

(1) Zhang, J.; Cheng, F.; Li, J.; Zhu, J.-J.; Lu, Y. Fluorescent nanoprobes for sensing and imaging of metal ions: Recent advances and future perspectives. *Nano Today* **2016**, *11* (3), 309−329.
(2) Etrych, T.; Janoušková, O.; Chytil, P. Fluorescence Imaging as a Tool in Preclinical Evaluation of Polymer-Based Nano-DDS Systems Intended for Cancer Treatment. *Pharmaceutics* **2019**, *11* (9), 471.
(3) Mandal, T.; Mishra, S. R.; Singh, K.; Agarwalla, H.; Masto, R. E.; Kumar, M.; Singh, V. Fluorescent carbon nanomaterials from coal and its derivatives: structure, properties, and applications. *J. Nanopart. Res.* **2023**, *25* (6), 125.
(4) Singh, V.; Rawat, K. S.; Mishra, S.; Baghel, T.; Fatima, S.; John, A. A.; Kalleti, N.; Singh, D.; Nazir, A.; Rath, S. K.; Goel, A. Biocompatible fluorescent carbon quantum dots prepared from beetroot extract for in vivo live imaging in C. elegans and BALB/c mice. *J. Mater. Chem. B* **2018**, *6* (20), 3366−3371.
(5) Singh, V.; Chatterjee, S.; Palecha, M.; Sen, P.; Ateeq, B.; Verma, V. Chickpea peel waste as sustainable precursor for synthesis of fluorescent carbon nanotubes for bioimaging application. *Carbon Letters* **2021**, *31* (1), 117−123.
(6) Rawat, K. S.; Singh, V.; Sharma, C. P.; Vyas, A.; Pandey, P.; Singh, J.; Gupta, N. M.; Sachdev, M.; Goel, A. Picomolar Detection of Lead Ions (Pb2+) by Functionally Modified Fluorescent Carbon Quantum Dots from Watermelon Juice and Their Imaging in Cancer Cells. *Journal of Imaging* **2023**, *9* (1), 19.
(7) Singh, V.; Mishra, A. K. Green and cost-effective fluorescent carbon nanoparticles for the selective and sensitive detection of iron (III) ions in aqueous solution: Mechanistic insights and cell line imaging studies. *Sens. Actuators, B* **2016**, *227*, 467−474.
(8) Bharathi, D.; Siddlingeshwar, B.; Krishna, R. H.; Singh, V.; Kottam, N.; Divakar, D. D.; Alkheraif, A. A. Green and Cost Effective Synthesis of Fluorescent Carbon Quantum Dots for Dopamine Detection. *J. Fluoresc.* **2018**, *28* (2), 573−579.
(9) Bharathi, D.; Krishna, R. H.; Singh, V.; Kottam, N.; Siddlingeshwar, B. One pot synthesis of C-dots and study on its interaction with nano ZnO through fluorescence quenching. *J. Lumin.* **2017**, *190*, 328−334.
(10) Singh, V.; Gorbel, B.; Chatterjee, S.; Sen, P.; Verma, V. Green, economical synthesis of nitrogen enriched carbon nanoparticles from seaweed extract and their application as invisible ink and fluorescent film. *Mater. Lett.* **2022**, *309*, No. 131446.
(11) Singh, V.; Mishra, A. K. White light emission from a mixture of pomegranate extract and carbon nanoparticles obtained from the extract. *Journal of Materials Chemistry C* **2016**, *4* (15), 3131−3137.
(12) Singh, V.; Mandal, T.; Mishra, S. R.; Singh, A.; Khare, P. Development of amine-functionalized fluorescent silica nanoparticles from coal fly ash as a sustainable source for nanofertilizer. *Sci. Rep.* **2024**, *14* (1), 3069.
(13) Mishra, M., Latest Trends in Bioimaging Using Quantum Dots. In *Smart Nanodevices for Point-of-Care Applications*; CRC Press: 2022; pp 135−142.
(14) Behera, L.; Mishra, L.; Mishra, M.; Mohapatra, S. Ca@Cu-CD nanoprobe for dual detection of glycine and ex vivo glycine imaging. *J. Mater. Chem. B* **2024**, *12*, 5181.
(15) Mohapatro, U.; Mishra, L.; Mishra, M.; Mohapatra, S. Zn-CD@Eu Ratiometric Fluorescent Probe for the Detection of Dipicolinic Acid, Uric Acid, and Ex Vivo Uric Acid Imaging. *Anal. Chem.* **2024**, *96*, 8630.
(16) Li, H.; Yan, X.; Kong, D.; Jin, R.; Sun, C.; Du, D.; Lin, Y.; Lu, G. Recent advances in carbon dots for bioimaging applications. *Nanoscale Horizons* **2020**, *5* (2), 218−234.
(17) Dalal, C.; Saini, D.; Garg, A. K.; Sonkar, S. K. Fluorescent Carbon Nano-onion as Bioimaging Probe. *ACS Applied Bio Materials* **2021**, *4* (1), 252−266.
(18) Priyadarsini, S.; Mohanty, S.; Mukherjee, S.; Basu, S.; Mishra, M. Graphene and graphene oxide as nanomaterials for medicine and biology application. *Journal of Nanostructure in Chemistry* **2018**, *8* (2), 123−137.
(19) Liu, F.; Jang, M.-H.; Ha, H. D.; Kim, J.-H.; Cho, Y.-H.; Seo, T. S. Facile synthetic method for pristine graphene quantum dots and graphene oxide quantum dots: origin of blue and green luminescence. *Adv. Mater.* **2013**, *25* (27), 3657−3662.
(20) Ahirwar, S.; Mallick, S.; Bahadur, D. Electrochemical Method To Prepare Graphene Quantum Dots and Graphene Oxide Quantum Dots. *ACS Omega* **2017**, *2* (11), 8343−8353.
(21) Yeh, T.-F.; Teng, C.-Y.; Chen, S.-J.; Teng, H. Nitrogen-Doped Graphene Oxide Quantum Dots as Photocatalysts for Overall Water-Splitting under Visible Light Illumination. *Adv. Mater.* **2014**, *26* (20), 3297−3303.
(22) Bradley, S. J.; Kroon, R.; Laufersky, G.; Röding, M.; Goreham, R. V.; Gschneidtner, T.; Schroeder, K.; Moth-Poulsen, K.; Andersson, M.; Nann, T. Heterogeneity in the fluorescence of graphene and graphene oxide quantum dots. *Microchimica Acta* **2017**, *184* (3), 871−878.
(23) Kang, S.; Kim, K. M.; Jung, K.; Son, Y.; Mhin, S.; Ryu, J. H.; Shim, K. B.; Lee, B.; Han, H.; Song, T. Graphene Oxide Quantum Dots Derived from Coal for Bioimaging: Facile and Green Approach. *Sci. Rep.* **2019**, *9* (1), 4101.
(24) Mirzoyan, Z.; Sollazzo, M.; Allocca, M.; Valenza, A. M.; Grifoni, D.; Bellosta, P. Drosophila melanogaster: A Model Organism to Study Cancer. *Front. Genet.* **2019**, *10*, 51.
(25) Ong, C.; Yung, L.-Y. L.; Cai, Y.; Bay, B.-H.; Baeg, G.-H. Drosophila melanogaster as a model organism to study nanotoxicity. *Nanotoxicology* **2015**, *9* (3), 396−403.
(26) Prüßing, K.; Voigt, A.; Schulz, J. B. Drosophila melanogaster as a model organism for Alzheimer's disease. *Mol. Neurodegener.* **2013**, *8* (1), 35.
(27) Liegeois, S.; Ferrandon, D. Sensing microbial infections in the Drosophila melanogaster genetic model organism. *Immunogenetics* **2022**, *74* (1), 35−62.
(28) Paithankar, J. G.; Kushalan, S.; S, N.; Hegde, S.; Kini, S.; Sharma, A. Systematic toxicity assessment of CdTe quantum dots in Drosophila melanogaster. *Chemosphere* **2022**, *295*, No. 133836.
(29) Alaraby, M.; Hernández, A.; Marcos, R. Novel insights into biodegradation, interaction, internalization and impacts of high-aspect-ratio TiO2 nanomaterials: A systematic in vivo study using Drosophila melanogaster. *Journal of Hazardous Materials* **2021**, *409*, No. 124474.
(30) Singh, A.; Raj, A.; Padmanabhan, A.; Shah, P.; Agrawal, N. Combating silver nanoparticle-mediated toxicity in Drosophila melanogaster with curcumin. *Journal of Applied Toxicology* **2021**, *41* (8), 1188−1199.
(31) Mandal, T.; Mishra, S. R.; Singh, V. Comprehensive advances in the synthesis, fluorescence mechanism and multifunctional applications of red-emitting carbon nanomaterials. *Nanoscale Advances* **2023**, *5* (21), 5717−5765.

(32) Mandal, T.; Ghosh, A. K.; Mishra, S. R.; Pandey, S. K.; Singh, V. Development of fluorescent carbon nanoparticles from Madhuca longifolia flower for the sensitive and selective detection of Cr6+: a collective experimental−computational approach. *Nanoscale Advances* **2023**, *5* (16), 4269−4285.
(33) Murmu, N.; Dash, K.; Panda, J.; Sahoo, G.; Sahoo, H.; Mishra, M.; Sahu, S. N. A biscoumarinyl hydrazone based nontoxic fluorescent dye for direct binding and imaging of actin in living cells and organism. *Sens. Actuators, B* **2024**, *399*, No. 134741.
(34) Nayak, P.; Bag, J.; Padhan, S. K.; Sahoo, H.; Sahu, S. N.; Mishra, M. Coumarin-Based Noncytotoxicity Fluorescent Dye for Tracking Actin Protein in In-Vivo Imaging. *Chem. Res. Toxicol.* **2023**, *36* (6), 926−933.
(35) Cheruku, R.; Bhaskaram, D. S.; Govindaraj, G. Variable range hopping and relaxation mechanism in graphene oxide sheets containing sp3 hybridization induced localization. *J. Mater. Sci.: Mater. Electron.* **2018**, *29*, 9663.
(36) Méndez-Lozano, N.; Pérez-Reynoso, F.; González-Gutiérrez, C. Eco-friendly approach for graphene oxide synthesis by Modified Hummers method. *Materials* **2022**, *15* (20), 7228.
(37) Fonseca, L. C.; de Araújo, M. M.; de Moraes, A. C. M.; da Silva, D. S.; Ferreira, A. G.; Franqui, L. S.; Martinez, D. S. T.; Alves, O. L. Nanocomposites based on graphene oxide and mesoporous silica nanoparticles: Preparation, characterization and nanobiointeractions with red blood cells and human plasma proteins. *Appl. Surf. Sci.* **2018**, *437*, 110−121.
(38) Thangaraj, B.; Mumtaz, F.; Abbas, Y.; Anjum, D. H.; Solomon, P. R.; Hassan, J. Synthesis of Graphene Oxide from Sugarcane Dry Leaves by Two-Stage Pyrolysis. *Molecules* **2023**, *28* (8), 3329.
(39) Naik, S.; Mishra, M., Exploration of Teratogenic and Genotoxic Effects on Model Organism Drosophila melanogaster. In *Teratogenicity Testing: Methods and Protocols*, Félix, L., Ed. Springer US: New York, NY, 2024; pp 317−330.
(40) Chauhan, S.; Naik, S.; Kumar, R.; Ruokolainen, J.; Kesari, K. K.; Mishra, M.; Gupta, P. K. In Vivo Toxicological Analysis of the ZnFe2O4@poly(tBGE-alt-PA) Nanocomposite: A Study on Fruit Fly. *ACS Omega* **2024**, *9* (6), 6549−6555.
(41) Shelke, T.; Rananaware, P.; Choudhary, N.; Naik, S.; Keri, R. S.; Brahmkhatri, V.; Mishra, M. Quercetin Nanoconjugates for Anti-Alzheimer's Activity: An Investigation on Drosophila melanogaster Model. *BioNanoScience* **2024**, 1.

https://doi.org/10.1021/acsomega.4c05244
ACS Omega 2024, 9, 38916−38924